Title

Reevaluation of a Bicyclic Pyrazoline as a Selective 15-Lipoxygenase V-Type Activator Possessing Fatty Acid Specificity

Journal

ACS Omega, 7(47)

ISSN

2470-1343

Authors

van Hoorebeke, Christopher
Yang, Kevin
Mussetter, Samuel J
et al.

Publication Date

2022-11-29

DOI

10.1021/acsomega.2c05877

ACS OMEGA

http://pubs.acs.org/journal/acsodf

Article

Reevaluation of a Bicyclic Pyrazoline as a Selective 15-Lipoxygenase V-Type Activator Possessing Fatty Acid Specificity

Christopher van Hoorebeke, Kevin Yang, Samuel J. Mussetter, Grant Koch, Natalie Rutz, R. Scott Lokey, Phillip Crews,* and Theodore R. Holman*

Cite This: *ACS Omega* 2022, 7, 43169−43179

Read Online

ACCESS | Metrics & More | Article Recommendations | Supporting Information

ABSTRACT: Regulation of lipoxygenase (LOX) activity is of great interest due to the involvement of the various LOX isoforms in the inflammatory process and hence many diseases. The bulk of investigations have centered around the discovery and design of inhibitors. However, the emerging understanding of the role of h15-LOX-1 in the resolution of inflammation provides a rationale for the development of activators as well. Bicyclic pyrazolines are known bioactive molecules that have been shown to display antibiotic and anti-inflammatory activities. In the current work, we reevaluated a previously discovered bicyclic pyrazoline h15-LOX-1 activator, PKUMDL_MH_1001 (written as **1** for this publication), and determined that it is inactive against other human LOX isozymes, h5-LOX, h12-LOX, and h15-LOX-2. Analytical characterization of **1** obtained in the final synthesis step identified it as a mixture of *cis*- and *trans*-diastereomers: *cis*-**1** (12%) and *trans*-**1** (88%); and kinetic analysis indicated similar potency between the two. Using compound **1** as the *cis*−*trans* mixture, h15-LOX-1 catalysis with arachidonic acid (AA) (AC_{50} = 7.8 +/− 1 μM, A_{max} = 240%) and linoleic acid (AC_{50} = 5.3 +/− 0.7 μM, A_{max} = 98%) was activated, but not with docosahexaenoic acid (DHA) or mono-oxylipins. Steady-state kinetics demonstrate V-type activation for **1**, with a β value of 2.2 +/− 0.4 and an K_x of 16 +/− 1 μM. Finally, it is demonstrated that the mechanism of activation for **1** is likely not due to decreasing substrate inhibition, as was postulated previously. **1** also did not affect the activity of the h15-LOX-1 selective inhibitor, ML351, nor did **1** affect the activity of allosteric effectors, such as 12*S*-hydroxy-5*Z*,8*Z*,10*E*,14*Z*-eicosatetraenoic acid (12S-HETE) and 14S-hydroperoxy-4*Z*,7*Z*,10*Z*,12*E*,16*Z*,19*Z*-docosahexaenoic acid (14S-HpDHA). These data confirm that **1** binds to a distinct activation binding site, as previously postulated. Future work should be aimed at the development of selective activators that are capable of activating h15-LOX-1 catalysis with DHA, thus enhancing the production of DHA-derived pro-resolution biomolecules.

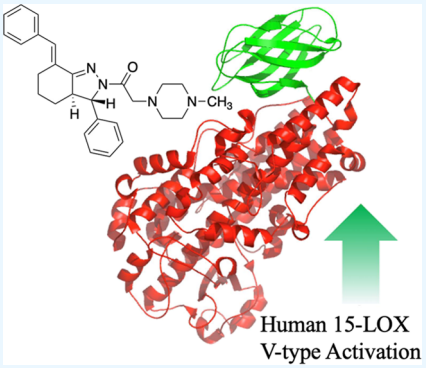

INTRODUCTION

Indazole-containing alkaloids are significant as they are continually being scrutinized for various pharmacological activities such as antitumor, anti-inflammatory, antioxidant, antiplatelet, anti-HIV, and anti-hypertensive.[1] Three types of indazole core structures are often explored for their anti-inflammatory pharmacology potential. An overview of key indazole constructs is shown in Figure 1, and specific examples of therapeutically significant compounds are shown in Figure 2. It is relevant to note that the fully aromatic 2*H*-indazole constitution represents the most stable member of these core structures. Based on this, the bioactivity evaluation of bicyclic pyrazoline (aka, hexahydro-2*H*-indazole) containing com-

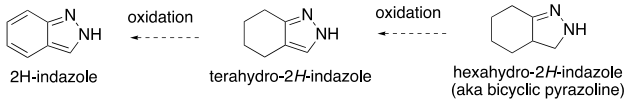

Figure 1. An overview of indazole core structures with potential as tools for anti-inflammatory pharmacology.

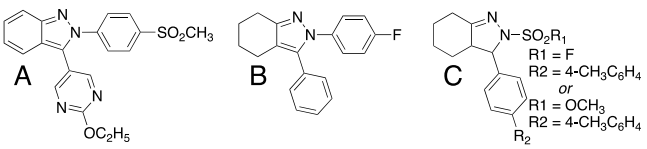

Figure 2. Indazole-containing compounds possessing anti-inflammatory potential or other relevant bioactivity properties. (A) 2*H*-indazole, COX-2 selective (IC_{50} = 409 nM);[2] (B) tetrahydro-2*H*-indazole, best of 18 analogues with COX-2 selectivity;[3] (C) hexahydro-2*H*-indazole, two best of 19 analogues with solid tumor cytotoxicity[4] and mild antibiotic activity.[5]

Received: September 10, 2022
Accepted: October 4, 2022
Published: November 17, 2022

https://doi.org/10.1021/acsomega.2c05877
ACS Omega 2022, 7, 43169−43179

pound libraries has been vigorously pursued, and a deep view into their properties can be found in two classic reports by independent medicinal chemistry teams.[6,7] Overall, these two works described 56 synthetic indazole alkaloids, including some with activity levels on a par with approved pharmaceuticals. One compound, from the 1979 report, possessed anti-inflammatory activity equivalent to that of (±) phenylbutazone[6] (Figure 3), a nonsteroidal anti-inflammatory

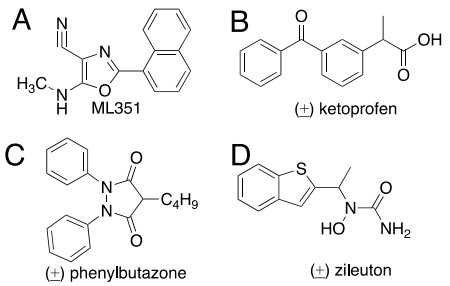

Figure 3. Molecular structures of anti-inflammatory tools and pharmaceutics. (A) ML351, h15-LOX-1 selective (IC_{50} = 200 nM); B) (±) ketoprofen, human NSAID therapeutic; (C) (±) phenylbutazone, animal NSAID therapeutic; and (D) (±) zileuton, human 5-LOX therapeutic.

drug (NSAID), and another molecule, described in 2003, possessed anti-inflammatory activity equivalent to that of the NSAID (±) ketoprofen[7] (Figure 3). It is important to underscore that a bicyclic pyrazoline was present in both these preceding active compounds. Additionally, a bicyclic pyrazoline core structure was also existent in a molecule examined by two different labs, first in 2016 as a putative human reticulocyte 15-LOX-1 (h15-LOX-1) activator[8] and then in 2017 as a low dose h15-LOX ferroptosis activator; this circumstance is discussed in more detail below. Described herein are experiments conducted to obtain next-generation understandings of bicyclic pyrazolines as potential bioactive substances affecting lipoxygenase (LOX), a significant contributor to inflammatory pathways.

As an important prelude, it is essential to briefly review the biological chemistry of human-lipoxygenases (h-LOX), non-heme iron enzymes that are ubiquitous in nature.[9,10] LOXs catalyze the dioxygenation of poly-unsaturated fatty acids (PUFA) containing at least one *cis*-1,4-pentadiene motif. In humans, there are four main human isoforms that have been extensively studied: h5-LOX,[11] h12-LOX,[12] h15-LOX-1,[13] and h15-LOX-2.[14] The nomenclature on this subject uses the substrate reaction specificity observed with arachidonic acid (AA), such as h15-LOX-1 producing 15-hydroperoxyeicosatetraenoic acid (15-HpETE). The metabolism of AA and other poly-unsaturated fatty acids (PUFAs) by LOX lead to both pro- and anti-inflammatory mono-oxylipin mediators, such as HETEs and HODEs, which are potent signaling mediators involved in a variety of outcomes during the complex inflammatory response.[15] Another dimension to this circumstance is that LOX isoforms are also involved in the development of both acute and chronic inflammation via the biosynthesis of di- or tri-hydroxylated PUFAs, such as lipoxins, maresins, resolvins, and protectins.[16−19] These small chiral molecules, known as specialized pro-resolving mediators (SPMs),[20] are also important cell signaling agents and are biosynthesized from PUFAs by: (a) LOXs, (b) cyclooxygenases (COXs), and/or (c) cytochrome P450 monooxygenases. Significantly, preclinical studies preliminarily implicate SPMs in orchestrating the perseverance of inflammation.[21]

The landscape for small-molecule LOX therapeutics to treat inflammation is sparse and continues to be focused on LOX specific inhibitors as tools to increase the understanding of experimental therapeutic strategies. Currently, (±) zileuton (Figure 3),[22] which targets h5-LOX, is the only FDA-approved LOX therapeutic. It is used for the treatment of asthma by decreasing the production of leukotrienes, pro-inflammatory molecules.[23] In addition, another low-nanomolar h15-LOX-1 inhibitor, ML351 (Figure 3), has been used to inhibit h15-LOX-1.[24] While these inhibitors have proven to be invaluable tools for understanding the role of LOX in cellular processes, another view on the understanding of the pro-resolution role of SPMs suggest that probing small-molecule LOXs activators could also guide more advanced studies on the role of LOX in biology. For example, allosteric regulation of human LOX during certain points of the inflammatory cascade could affect its perseverance, thereby lowering the level of inflammation.[25]

Interestingly, until recently, there have been no published synthetic small molecules which allosterically activated LOX catalysis. In this context, the results described in 2016 and 2017 provided data demonstrating the use of synthetic bicyclic pyrazolines to increase the rate of h15-LOX-1 production of inflammatory lipid mediators.[8,26] Taken together, the outcomes of these studies are intriguing and support the conclusion that bicyclic pyrazolines are capable of activating h15-LOX-1. Conversely, several chemical/biochemical details were lacking in the design of these past studies. Examples of lingering questions include (a) the NMR/MS data to support a rigorous structural assignment of the bicyclic pyrazoline was incomplete, (b) the possibility of observing LOX and/or fatty acid specificity was not explored, (c) defining the allosteric site assessment was not discussed, and (d) detailed experiments probing kinetic data to fully understand a steady-state mechanism were missing. Thus, a project was launched to answer these questions and at the same time obtain a comprehensive understanding of the chemical, biochemical, and kinetic properties imparted by this bicyclic pyrazoline activator on h15-LOX-1. Ultimately, the results presented below will be of value in defining the constraints of subsequent in vivo experiments.

METHODS

Expression and Purification of h5-LOX, h12-LOX, h15-LOX-1, and h15-LOX-2. Overexpression and purification of wild-type (wt) h15-LOX-1 (Uniprot entry P16050),[27,28] h12-LOX (Uniprot entry P09917),[27,28] h5-LOX (Uniprot entry P09917),[29] and h15-LOX-2 (Uniprot entry O15296)[30] were performed as previously described. A nickel-NTA chromatography system at 4 °C was used to purify His-tag labeled h12-LOX, h15-LOX-1, and h15-LOX-2. The purity of h15-LOX-1, h15-LOX-2, and h12-LOX was assessed by sodium dodecyl sulfate-polyacrylamide gel electrophoresis (SDS-PAGE) to be >90%. The metal content was assessed on a Finnigan inductively coupled plasma mass spectrometer (ICP-MS), via comparison with an iron standard solution. Cobalt-EDTA was used as an internal standard. The h5-LOX was not purified due to a dramatic loss of activity and was prepared as an ammonium sulfate precipitate.

Synthesis of 1-[(7*E*)-7-Benzylidene-3-phenyl-3*a*,4,5,6-tetrahydro-3*H*-indazol-2-yl]-2-(4-methylpiperazin-1-yl)-

https://doi.org/10.1021/acsomega.2c05877
ACS Omega 2022, 7, 43169−43179

Scheme 1. Preparation of 1 (aka PKUMDL_MH_1001) as a Mixture of Isomers[26]

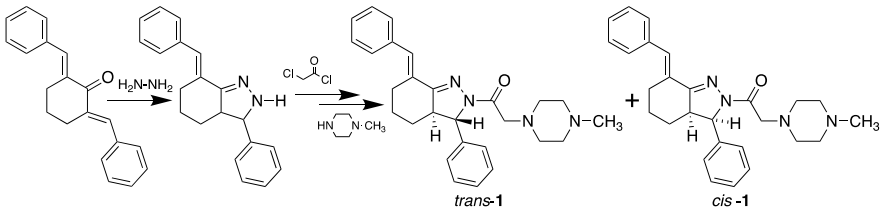

ethenone] and Purification of the *trans* and *cis* Diasteromers. The *trans*−*cis* isomer mixture of compound **1** was synthesized according to published procedure (Supporting Information, Scheme S1),[26] and the bicyclization step, shown in Scheme 1, generated a racemic mixture of the two diastereomers. The final purification step afforded pure *trans*-**1** and *cis*-**1**, the latter being more unstable than the former. It should be noted that if not specifically indicated herein, the term **1** refers to the mixture of *trans*-1 and *cis*-1. The purification steps used high-pressure liquid chromatography (HPLC) on a Higgins Haisil semi-preparative (5 μm, 250 mm × 10 mm) C18 column with a 95:5 to 5:95 gradient of water and ACN, both with 0.1% (v/v) formic acid (FA) over 70 min and a flow rate of 2 mL/min.

1-[(7*E*)-7-Benzylidene-3-phenyl-3*a*,4,5,6-tetrahydro-3*H*-indazol-2-yl]-2-(4-methylpiperazin-1-yl)ethenone]. ^{1}H NMR (800 MHz, $CDCl_3$) δ 7.36 (m, 7H), 7.29 (tt, 1H), 7.25 (d, 2H), 7.18 (d, 1H), 4.89 (d, 1H), 3.72 (s, 2H), 3.06 (d bm, 1H), 2.97 (ddd, 1H), 2.78 (bs, 8H), 2.44 (s, 3H), 2.43 (ddd, 1H), 2.21 (ddd, 1H), 1.93 (ddd, 1H), 1.69 (qd, 1H), 1.47 (qt, 1H). ^{13}C NMR (500 MHz, d_8-DMSO) δ168.5, 158.7, 142.2, 135.7, 130.9, 129.7, 129.7, 128.8, 128.6, 127.9, 127.2, 125.7, 67.4, 58.9, 56.3, 54.7, 52.6, 45.8, 29.2, 28.7, 23.7 (Figure 4, Table 1). HRMS *m*/*z* 429.2651 [M$^+$H] (calculated for

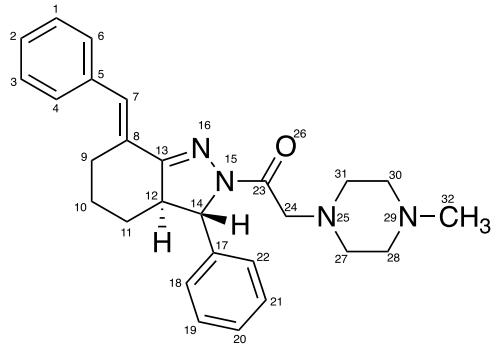

Figure 4. *Trans*-**1** (aka PKUMDL_MH_1001).

$C_{27}H_{33}N_4O^+$, 429.2649). See Supporting Information for NMR of **1** (Figures S1 and S2), comparison to literature spectra (Figures S3 and S4)[26] and MS spectra (Figure 6 and Figure 7).

***Cis*−*Trans* Identification via Molecular Mechanics Computation of 1.** Compound **1** has two stereocenters at C12 and C14 that constitute *trans*-**1** and *cis*-**1** isomers (Scheme 1), which were not characterized or separated in previous studies.[8,26,31] Molecular modeling, using Chem3D 20.1 (Figure 5), helped to establish the identity of the two isomers. Each diastereomer was energy-minimized using the MM2 forcefield, and the dihedral angle H(C12)−H(C14) was calculated for the lowest energy conformers of each diastereomer. Next, these data were input into the Karplus equation[32] to calculate *J*-values for each diastereomer, and subsequently compared to the experimental *J*-values (Supporting Information, Figures S5 and S6).[6,33] The comparisons between the *J*-values from each Karplus equation calculation and the experimental NMR data indicate that the relative stereochemistry of the major isomer of **1** obtained from synthesis can be confidently assigned as *trans* (Supporting Information, Figures S5 and S6).[6,33]

LC−MS/MS Analysis of 1. The mixture of the final reaction product **1** was verified in part through liquid chromatography coupled with electrospray-ionization tandem mass spectrometry (LC/ESI-MS/MS). Chromatographic separation of the two diastereomers, *cis*-1 and *trans*-1, was performed on a Dionex UltiMate 3000 UHPLC with a C_{18} column (MAC-MOD, ACE Excel 5 μm, 250 mm × 4.6 mm). The autosampler was held at 4 °C, and the injection volume was 20 μL. Mobile phase A consisted of H_2O with 0.1% (v/v) FA, and mobile phase B consisted of acetonitrile with 0.1% FA. The flow rate was 1.0 mL/min. The initial condition (5% mobile phase B) was held for 2 min and then ramped up to 95% over 10 min. Mobile phase B was held at 95% for an additional 3 min. The chromatography system was coupled to an Orbitrap Velos Pro (Thermo Scientific) for mass analysis. Analytes were ionized via heated electrospray ionization with 4.0 kV spray voltage and 35, 10, and 0 arbitrary units for sheath, auxiliary, and sweep gas, respectively. The radio-frequency amplitude of the S-Lens was 65%, and the probe and capillary temperatures were 45 and 380 °C, respectively. All analyses were performed in positive ionization mode at the high-resolution setting (100,000). MS^2 was performed in the ion trap with a normal scan rate at 35% normalized collision energy in a targeted manner with a mass list containing the following *m*/*z* ratios ±0.3: 429.265 (**1**) and its fragments, 329.165, 301.170, 244.144, and 141.102 (Figures 6 and 7).

Specificity of 1 with LOX Isozymes and Fatty Acids and Oxylipin Substrates. Compound **1** was screened to determine its activation specificity against human LOXs. It should be noted that these bicyclic pyrazolines are unstable, the NMR spectra of *trans*-**1** indicated it was stable to prolonged storage (Figure 1),[34] but this was not the case for *cis*-**1**. Subsequently, all biological assays were performed with freshly dissolved solids and stored on ice. h15-LOX-1 and h15-LOX-2 reactions were performed in 25 mM HEPES (pH 7.5), while h12-LOX reactions were carried out in 25 mM HEPES (pH 8.0). Reactions with the crude, ammonium sulfate-precipitated h5-LOX were carried out in 25 mM HEPES (pH 7.3), 0.3 mM $CaCl_2$, 0.1 mM EDTA, and 0.2 mM ATP. All isoforms were screened at 10 μM **1**, 10 μM AA, and 0.01% Triton X-100. 15S-HpETE formation rates were determined by the increase in absorbance at 234 nm (ϵ_{234nm} = 27,000 M^{-1} cm^{-1}), with the concentration of AA being determined by measuring the amount of 15S-HpETE produced from the complete reaction with soybean lipoxygenase-1 (sLO-1). Rate

https://doi.org/10.1021/acsomega.2c05877
ACS Omega 2022, 7, 43169−43179

Table 1. ^{1}H (800 MHz, $CDCl_3$) and ^{13}C (125 MHz, DMSO-d_6) Data for *trans*-1 (aka PKUMDL_MH_1001), Shown in Figure 4[a]

pos.	δ_C, type	δ_H, J (Hz)	COSY	NOESY
1	129.7, CH	7.36, m	2, 6	
2	125.7, CH	7.36, m	1, 3	
3	129.7, CH	7.36, m	2, 4	
4	127.2, CH	7.36, m	3	
5	130.9, C			
6	127.2, CH	7.36, m	1	
7	127.9, CH	7.18, d (1.5)	9b	
8	135.7, C			
9a	28.7, CH_2	3.06, bd (15.1)	9b, 10a, 10b	$9b^s$, $10a^m$, $10b^m$
9b	28.7, CH_2	2.43, ddd (13.0,5.6,2.9)	9a, 10a, 10b	$9a^s$, $10b^m$, $11b^w$
10a	23.7, CH_2	1.47 qt (12.8, 3.8)	9a, 9b, 10b, 11a, 11b	$9a^m$, $10b^s$, $11a^m$, 12^m
10b	23.7, CH_2	1.93, ddd (13.7,5.2,2.3)	9a, 9b, 10a, 11a, 11b	$9a^w$, $9b^m$, $10a^s$, $11a^m$, $11b^m$
11a	29.2, CH_2	2.21, ddd (12.7,4.2,2.2)	12, 10a, 10b, 11b	$10a^m$, $10b^m$, $11b^s$, 12^m
11b	29.2, CH_2	1.69, qd (12.9, 2.9)	12, 10a, 10b, 11a	$9b^w$, $10b^w$, $11a^s$, 12^w, 14^m
12	56.3, CH	2.97, ddd (9.4,6.5,5.8)	14, 11a, 11b	$10a^m$, $11a^m$, 14^w
13	158.7, C			
14	67.4, CH	4.89, d (9.4)	12	$11a^w$, $11b^m$, 12^w
17	142.2, C			
18	128.8, CH	7.25, d (7.0)	19	
19	128.6, CH	7.36, m	18, 20	
20	125.7, CH	7.29, tt (7,2)	19, 21	
21	128.6, CH	7.36, m	20, 22	
22	128.8, CH	7.25, d (7.0)	21	
23	168.5, C			
24	58.9, CH_2	3.72, s		27^m,31^m
27	52.6, CH_2	2.78, bm		24^m
28	54.7, CH_2	2.78, bm		
30	54.7, CH_2	2.78, bm		
31	52.6, CH_2	2.78, bm		24^m
32	45.8, CH3	2.44, s		

[a]s = strong NOE, m = medium NOE, and w = weak NOE.

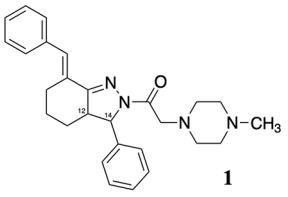

1

	J_{exp} (Hz)	J_{calc} (Hz)	DH_{calc} (deg)
trans	9.4	9.4	158
cis		7.3	26

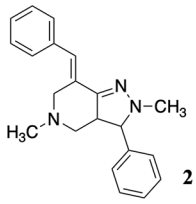

2

	J_{exp} (Hz)[i]	J_{calc} (Hz)	DH_{calc} (deg)
trans	13	10.3	170
cis	-	6.2	36

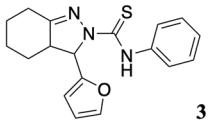

3

	J_{exp} (Hz)[ii]	J_{calc} (Hz)	DH_{calc} (deg)
trans	5	5.6	131
cis	11	8.6	2

Figure 5. Diagnostic $^{3}J_{HH}$ and dihedral angle (DH) values between H12−H14 to track *trans*/*cis* orientations in bicyclic pyrazolines; **1**, **2**,[6] and **3**.[33]

enhancement of h15-LOX-1 by **1** was also determined with 15S-HpETE as substrate. Reactions were carried out in 25 mM HEPES (pH 7.5), 0.01% Triton X-100, and 10 μM for **1**, with concentrations varying for 15S-HpETE (e.g., 5, 10, and 20 μM). Following the addition of enzyme, the substrate turnover was monitored at 270 nm (conjugated triene) for the creation of diHpETEs (ε_{270nm} = 37,000 M^{-1} cm^{-1}). All reactions were performed in duplicate at an ambient temperature under constant stirring. The reactions were initiated by the addition of enzyme and were monitored on a Perkin−Elmer Lambda 45 UV/VIS spectrophotometer. Simultaneous reactions were run in the absence of **1** for all reactions to determine the increase in maximal rate. Error values are reported based on the saturation curve fits.

Kinetic Analysis of 1 and AC_{50} Determination with h15-LOX-1. h15-LOX-1 reactions were performed, at an ambient temperature, constantly stirred with a magnetic stir bar in a 1 cm^2 quartz cuvette containing 2 mL of 25 mM HEPES (pH 7.5), 0.01% Triton X-100, and substrate in the presence and absence of **1**. The AA concentration was varied from 0.74 to 19.3 μM, while the concentration of **1** was held constant (four separate experiments of 0, 5, 20, and 30 μM of **1**). AC_{50} investigations were performed at 10 μM substrate (AA, DHA, or LA) and concentrations of **1** ranging from 0.5 to 100 μM. The AC_{50} for the purified *trans*-1 and *cis*-1 isomers were also determined (see Figure S7). An AC_{50} assay utilizing the buffer conditions of the discovering lab[8] was also performed, 100 mM PBS (pH 7.4) and 1% DMSO. UV

https://doi.org/10.1021/acsomega.2c05877
ACS Omega 2022, 7, 43169−43179

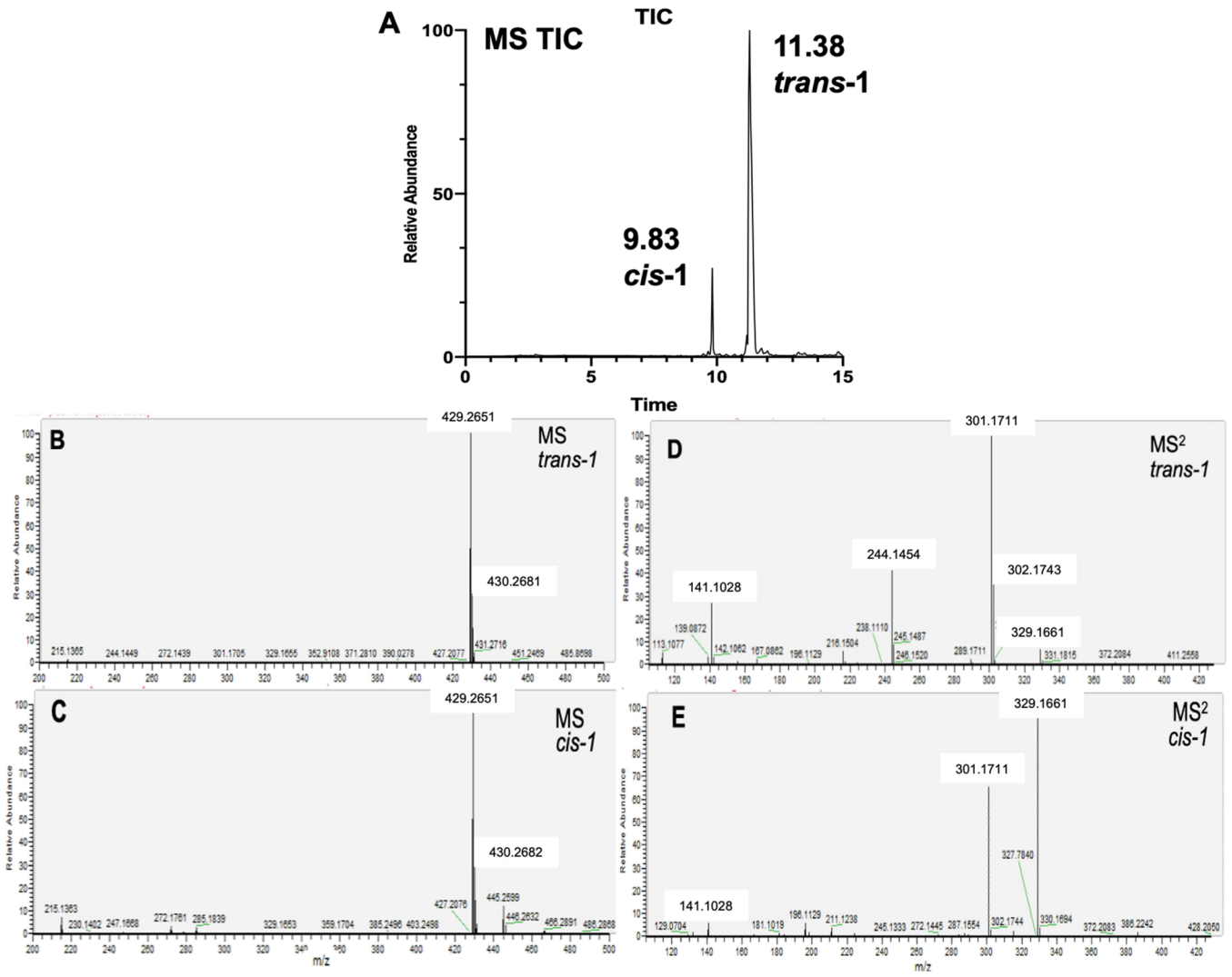

Figure 6. LC−MS/MS data for *cis*-**1** and *trans*-**1**. (A) LC−MS TIC trace showing minor peak (*cis*-**1**) at 9.83 min (12%) and major peak (*trans*-**1**) at 11.38 min (88%). (B) *trans*-**1**, Parent ion of MS TIC peak at 11.38 min. (C) *cis*-**1**, Parent ion of MS TIC peak at 9.83 min. (D) *trans*-**1**, MS^2 fragments for 11.38 min after the 429.3 mass filter was applied. (E) *cis*-**1**, MS^2 fragments for 9.83 min after the 429.3 mass filter was applied.

KinLab (Perkin−Elmer) was used to fit initial rates, and KaleidaGraph (Synergy) was used to determine the kinetic parameter (k_{cat}/K_M) to the Michaelis−Menten equation for the calculation of kinetic parameters. The activation rates were determined by subtracting the rate of the vehicle (DMSO) reaction from the rate of the reaction with **1**. AC_{50} values were obtained by determining the % change in the enzymatic rate, relative to vehicle control, at seven activator concentrations, and plotting them against the activator concentration. The data were fit using a four-parameter, variable slope analysis normalized with R_{MAX} = 100%. Reactions were initiated through the addition of enzyme (∼60 nM final concentration). The data used for the saturation curve fits were performed in triplicate. Error values are reported based on the kinetic and saturation curve fits.

h15-LOX-1 Product Profile in the Presence of 1. Product profile reactions were carried out in a similar manner as the kinetic reactions detailed above except no Triton X-100 was added. Reactions were quenched with the addition of 3% glacial acetic acid, washed 3× with 2 mL DCM, reduced with a drop of trimethylphosphite, evaporated under a stream of N_2 gas, reconstituted in a 1:1 mixture of ACN and H_2O with 0.1% FA, and injected on a Dionex UltiMate 3000 UHPLC with a C_{18} column (Phenomenex Kinetex, 1.7 μm, 150 mm × 2.1 mm) coupled to an Orbitrap Velos Pro (Thermo Scientific) for product analysis. Mobile phase A consisted of water with 0.1% (v/v) FA, and mobile phase B consisted of acetonitrile with 0.1% FA. The flow rate was 0.2 mL/min. The initial condition (50% mobile phase B) was held for 1 min and then ramped up to 75% over 16 min. Mobile phase B was held at 75% for an additional 9 min. Analytes were ionized via heated electrospray ionization with −4.0 kV spray voltage and 35, 10, and 0 arbitrary units for sheath, auxiliary, and sweep gas, respectively. The radiofrequency amplitude of the S-Lens was 65%, and the probe and capillary temperatures were 45 and 380 °C, respectively. All analyses were performed in negative ionization mode at the normal resolution setting. MS^2 was performed at 35% normalized collision energy in a targeted manner with a mass list containing the following m/z ratios ±0.1: 319.2 (HETE) and 335.2 (diHETE).

Substrate Inhibition and Lag Phase Investigations in the Presence of 1. Initial rate screening was carried out to determine the capacity of **1** to lower the inhibitory effects of high substrate concentrations on h15-LOX-1.[35] The reactions

https://doi.org/10.1021/acsomega.2c05877
ACS Omega 2022, 7, 43169−43179

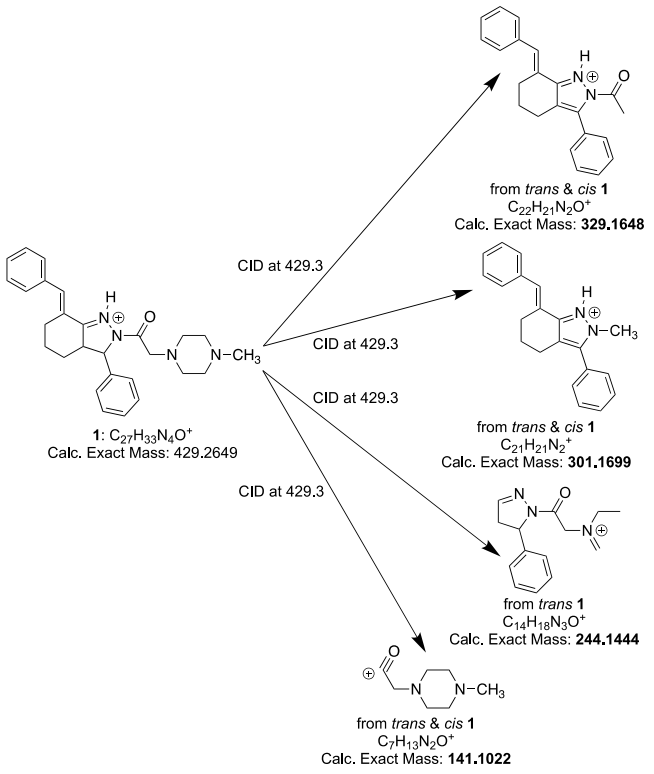

Figure 7. Proposed (+ ion) MS/MS fragmentation of **1** (*trans* or *cis*) from CID at 429.3.

were carried out at an ambient temperature and constantly stirred with a magnetic stir bar in a 1 cm^2 quartz cuvette containing 2 mL of 25 mM HEPES (pH 7.5) and 0.01% Triton X-100. The substrate, DHA and AA, concentrations varied from 25, 50, and 100 μM while the activator concentration was held constant at 10 μM. Additional experiments were performed to investigate if the activator altered the affinity of substrates to the ferrous form of h15-LOX-1, as has been previously investigated.[35] Reactions were conducted as described for the steady-state experiments above, initiating the assays by adding h15-LOX-1, final concentration of ~60 nM, to buffers containing LA, AA, or DHA under substrate limiting conditions (5 μM). Lag phases, the time difference from reaction initiation to a maximal rate, and V_0, were recorded. Reactions were run in triplicate and standard deviation values reported based on triplicate runs.

Inhibition Potential of ML351 in the Presence of 1. The inhibition potential of the selective, potent h15-LOX-1 inhibitor, ML351,[24] was determined in the presence of **1**. Reaction rates were determined by following the formation of the conjugated diene product, 15-HpETE, at 234 nm with a Perkin−Elmer Lambda 40 UV/Vis spectrophotometer at five inhibitor concentrations with and without the presence of 10 μM of **1**. All reaction mixtures were 2 mL in volume and constantly stirred using a magnetic stir bar at an ambient temperature with the appropriate amount of h15-LOX-1, ~60 nM. All the reactions were carried out in 25 mM HEPES buffer (pH 7.5), 0.01% Triton X-100, and 10 μM AA. The concentration of AA was quantitated by allowing the reaction to go to completion with sLO-1. IC_{50} values were obtained by plotting the initial reaction rates against the inhibitor concentration, followed by a hyperbolic saturation curve fit. The data used for the saturation curve fits were performed in triplicate and the error values reported.

Impact of 1 on Allosteric Modulators of h15-LOX-1. The negative allosteric modulator, the 14S-hydroperoxy-4Z,7Z,10Z,12E,16Z,19Z-docosahexaenoic acid (14S-HpDHA), was varied from 1 to 100 μM in the presence and absence of 10 μM of **1** to determine whether **1** altered the allosteric effect of 14S-HpDHA. The concentration of the 12S-hydroxy-5Z,8Z,10E,14Z-eicosatetraenoic acid (12S-HETE) was also varied (0.1 to 5 μM), with a 1 μM, 1:1 LA and AA mixture as substrate. **1** (10 μM) was added to determine if it altered the allosteric effect of 12S-HETE. The product profile reactions and extractions were carried out as mentioned above. MS^2 was performed at 35% normalized collision energy in a targeted manner with a mass list containing the following m/z ratios ±0.1: 295.2 (HODE), 319.2 (HETE), and 359.2 (diHDHA).

RESULTS AND DISCUSSION

Characterization and Stereostructural Analyses of Bicyclic Pyrazolines. As discussed above, the findings that compound **1**, previously named PKUMDL_MH_1001,[8,26,31] was an h15-LOX-1 activator was exciting and merited follow up. The SAR activity data also described in both the open and patent literature indicated that a bicyclic pyrazoline moiety was essential to observing this and other interesting pharmacological effects.[8,26,31,36] Thus, the first step in this project involved adopting previously described procedures,[6,26,34] to prepare **1** (Supporting Information, Scheme S1).

The successive set of reactions shown in Scheme 1 afforded crude material of **1** in high yield (57%). Moreover, the key bicyclization step was expected to afford a mixture of *trans*/*cis* products as precursors for subsequent conversion to **1**. Eventual separation of the final reaction product (0.4 g) by semi-preparative HPLC yielded two products, rt = 9.83 min (12%) and rt = 11.38 min (88%), that were next evaluated by accurate LC-MS^2 data, as shown in Figures 6 and 7. These analyses indicated that diastereomers were obtained that possessed identical MH^+ m/z = 429.2654 for a calculated MF = $C_{27}H_{33}N_4O^+$ (unsat. = 14). The MS/MS multiple reaction monitoring by CID (pos. ion) at m/z 429.3 for each compound also revealed an array of diagnostic major fragment ion peaks (among the collection of m/z: 329.165/301.170/244.144/141.102). Initial 15-LOX activator measurements were carried out on this reaction product mixture and some of the subsequent analyses employed the purified major component. It is important to note that all previous published pharmacologic investigations on **1** appeared to utilize mixtures.[8,26,31] Thus, some of the goals in this work included (a) a rigorous definition of the stereo-structures of the isomer mixture obtained from Scheme 1, (b) an assessment of the stability of the material used in the screening work, (c) a beginning assessment of the relative pharmacological activity of the **1** isomers, and (d) a forecast of the possibility that better bioactive bicyclic pyrazoline analogues could be designed.

From the outset, it was important to complete a rigorous evaluation of the NMR data for *trans*-**1**, as this was lacking in the literature.[8] The results for the major isomer assigned as having a *trans* configuration at C-12/C-14 are shown in Table 1. The fully annotated NMR spectra displayed distinct signals for all 27 carbons and 32 hydrogens distributed about the five rings (two phenyl, a bicyclic pyrazoline, and an *N*-methylpiperazine). Moreover, all their δ and *J*-values were

https://doi.org/10.1021/acsomega.2c05877
ACS Omega 2022, 7, 43169−43179

rigorously assigned using the 2D NMR data shown in the Supporting Information (Figure S2). The additional unsaturation functionality was pinpointed by other NMR resonances at: (a) $\delta_{H\text{-}7}$ = 7.18 (d = 1.5 Hz), $\delta_{C\text{-}7}$ = 127.9, $\delta_{C\text{-}8}$ = 135.7, and $\delta_{C\text{-}13}$ = 158.7; and (b) $\delta_{H\text{-}24}$ = 3.72 (s), $\delta_{C\text{-}24}$ = 58.9, and $\delta_{C\text{-}23}$ = 168.5. Attempts to annotate the NMR data obtained (not shown herein) for the minor isomer assumed to be *cis* were not possible because it contained many spurious signals, presumably due to its decomposition during sample storage. By contrast the MS/MS spectra of the *cis* isomer looked clean (data not shown).

The final assignment of the major **1** isomer as *trans*-**1** was based on the variation in the $^3J_{H\text{-}14/H\text{-}12}$. It was assumed that the variation in the corresponding HC-14/HC-12 dihedral angles should provide diagnostic data to distinguish between the *trans* vs *cis* configurations. This postulation was validated through a side-by-side comparison of experimental J's vs those calculated from the computer-driven molecular modeling (Figure 5) and some trends are as follows. (a) The *trans*-**1** configuration of the major compound was assigned by comparing the experimental $^3J_{14-12}$ vs that calculated during the molecular modeling runs (Supporting Information, Figures S5 and S6). (b) The experimental $^3J_{14-12}$ = 9.4 Hz was identical to that calculated (9.4 Hz) for *trans*-**1** and different to that calculated for *cis*-**1** (7.1 Hz) during molecular modeling and Karplus equation analysis of the dihedral angles measured (trans = 158° vs *cis* = 26°). Other vicinal J's measured showed that the rigid 6-membered ring possessed a chair conformation indicted by proximal bis-axial protons: (i) H9a/H10a (^3J = 12.8 Hz), (ii) H10a/H11b (^3J = 12.8 Hz), and (iii) H11b/H12 (^3J = 12.9 Hz). The co-planarity of bis-axial H10a and 12 was also indicated by their respective medium NOESY correlations (Supporting Information, Figure S2). Returning to the significance of J-ratios to assess trans−cis assignments; the above trend *trans* > *cis* is also observed in the data for **2** (Figure 5). In this case, the experimental value for the *trans*-**1**, $^3J_{14-12}$ = 13 Hz,[6] is close to that calculated (10.3 Hz) and distant to that calculated for *cis* (6.2 Hz). Another noteworthy fact is that the replacement of CH_2 at C-11 in **1** by *N*-CH_3 in **2** has a measurable impact but does not alter the J trend *trans* > *cis*. However, an opposite pattern is observed for compound **3** in which $^3J_{14-12}$ *cis* > *trans* for both the experimental and calculated data, reflecting a change in the six membered ring conformation mediated by the lack of an exocyclic methylene moiety at position C-8. Additional insights on the variations in the diagnostic J-ratios were explored by additional in silico modeling on 15 bicyclic pyrazoline analogues with varying double bonds present or absent at different positions in the cyclohexane ring of the bicyclic pyrazoline core (Supporting Information, Figures S5 and S6). Overall, 53% of this collection showed $^3J_{14-12}$ *trans* > *cis*.

Specificity of 1 with LOX Isozymes and Fatty Acids and Oxylipin Substrates. Compound **1**, defined as the mixture of *trans/cis*, was screened at 10 and 20 μM against h5-LOX, h12-LOX, h15-LOX-1, and h15-LOX-2, to determine the specificity of the activator for h-LOXs. It was determined that only h15-LOX-1 had an increased rate, 67% at 10 μM, in the presence of **1** (Table 2), with the remaining hLOX isoforms displaying mild, dose-independent inhibition, indicating that **1** is a h15-LOX-1 specific activator. With confirmation that **1** selectively activates h15-LOX-1 against AA catalysis, the role of **1** with 15S-HpETE as the substrate was investigated, however, no activation was observed. This indicates that activation by **1** is specific for the reaction of h15-LOX-1 with AA but not the oxylipin 15S-HpETE, which may have implications for the use of **1** in vivo since h15-LOX-1 must react with oxylipins in order to form some SPM. Interestingly, the AC_{50} for the two isolated diastereomers, *cis*-**1** and *trans*-**1**, were determined to be similar and therefore all subsequent experiments utilized the isomeric mixture of **1** (Supporting information, Figure S7). However, it should be noted that while the peaks were resolved via LCMS, the NMR spectra of *cis*-**1** indicated an impure sample hours after its solubilization in solvent.

Table 2. Activator Specificity (1) versus h5-LOX, h12-LOX, h15-LOX-1, and h15-LOX-2 with AA as the Substrate[a]

enz	0 μM of **1**	10 μM of **1**	20 μM of **1**
h5-LOX	100(1) %	78(1) %	91.3(1) %
h12-LOX	100(1) %	75(1) %	83.3(1) %
h15-LOX-1	100(1) %	167(1) %	212(2) %
h15-LOX-2	100(1) %	74.4(1) %	94.9(1) %

[a]Initial rates, measured as dA/s, are presented as a percentage, with 0 μM activator reactions set to 100%. The error is displayed in parentheses.

AC_{50} Determination of 1 with h15-LOX-1. Following the determination that **1** was specific for h15-LOX-1, the AC_{50} with LA, AA, and DHA was determined to better understand the substrate specificity of **1**. The reaction of h15-LOX-1 with LA (C18:2 poly-unsaturated fatty acid (PUFA)) and AA (C20:4 PUFA) was activated in the presence of **1** (Figure 8, Table 3), with the AC_{50} for LA being 5.3 +/− 0.7 μM (98% max activation) and 7.8 +/− 1 μM for AA (240% max activation). It should be noted that the AC_{50} value for AA is comparable to that observed by Meng et al.[8] (AC_{50} value = 6.8 +/− 0.4 μM, max activation = 85%); however, these conditions are distinct from that of Meng et al. When we

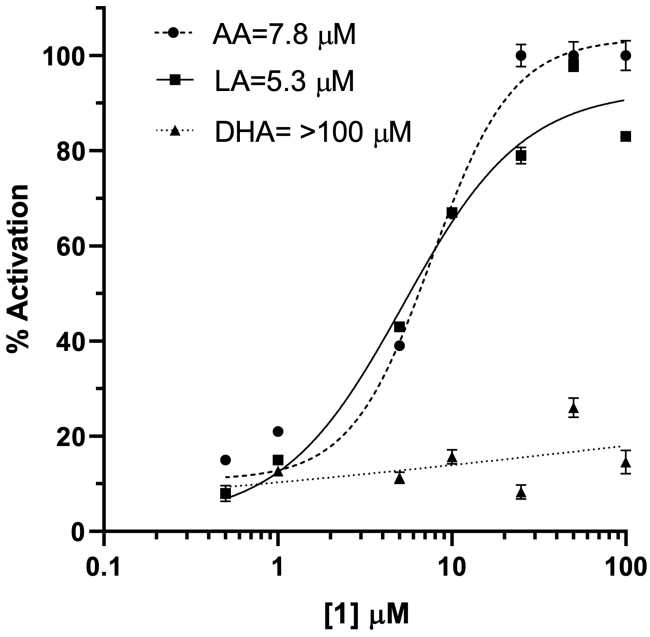

Figure 8. The saturation curves are shown of compound **1** with various substrates. The calculated AC_{50} values (μM) were determined with LA (squares, AC_{50} = 5.3 +/− 0.7 μM), AA (circles, AC_{50} = 7.8 +/− 1 μM), and DHA (triangles, AC_{50} > 100 μM).

https://doi.org/10.1021/acsomega.2c05877
ACS Omega 2022, 7, 43169−43179

Table 3. AC_{50} Values (μM) and Max Activation % at Different PUFA Concentrations[a]

AC_{50} kinetics	10 μM PUFA	50 μM PUFA	50 μM[b] PUFA
AA	7.8 (1) μM, 240 (20) %	3.8 (0.6) μM, 190 (10) %	9.7 (1) μM, 150 (7) %
LA	5.3 (0.7) μM, 98 (9) %	ND	ND
DHA	>100 μM, 26 (10) %	ND	ND

[a]ND = not determined. [b]This AC50 value was determined using the buffer conditions from ref 8, however with stirring. The lack of stirring increased the AC_{50} significantly. The error is displayed in parentheses.

attempted to reproduce their work under the published conditions, a reliable AC_{50} could not be obtained. As has been published previously,[37,38] the absence of stirring can lead to variable LOX rates, which we observed under the conditions of Meng et al.[8] Gratifyingly, with constant stirring and initiation of the reaction by enzyme addition, an AC_{50} of 9.7 +/− 1 μM (150% max activation) at 50 μM AA was obtained with the Meng et al.[8] buffer conditions (Table 3), which is comparable to the published value. Finally, the reaction rate of h15-LOX-1 with DHA, a C22:6 PUFA, was not activated with **1**, up to 100 μM (Figure 8). These data indicate that the activation of h15-LOX-1 by **1** is dependent on the nature of the PUFA substrate, with LA and AA being activated; however, DHA is not. The lack of DHA activation has relevancy concerning **1** as a cellular tool since DHA is one of the main SPM precursors.

Lag Phase and Substrate Inhibition in the Presence of 1. Previous studies have suggested that part of the kinetic activation potential of **1** was derived from its ability to lower the effect of substrate inhibition on h15-LOX-1.[8,31] To further shed light on this hypothesis, lag phase experiments at high substrate concentration were carried out because the lag phase observed for LOX reactions is partially due to substrate binding to the inactive ferrous form.[35] Given this, it was observed that the h15-LOX-1 lag phase was reduced by 140 s with the activator (25 μM AA), with a 98% rate increase (Table 4 and Figure 9). This reduced lag phase and increased rate were decreased slightly with increasing substrate concentration, 50 and 100 μM AA. With DHA, the lag phase decreased by nearly 200 s, but the rate only increased by 25% at 100 μM AA. Taken together, these data indicate that while **1** does lower lag phase and hence the affinity of AA and DHA to the ferrous form of h15-LOX-1, this effect does not account for enzyme activation since DHA catalysis is not enhanced.

Table 4. Substrate Inhibition Determination in the Presence of Activator, Compound 1[a]

arachidonic acid	25 μM	50 μM	100 μM
Δlag phase (s)	140 (10) s	93 (6) s	110 (20) s
% rate increase	98 (3) %	71 (7) %	30 (12) %
docosahexaenoic acid	25 μM	50 μM	100 μM
Δlag phase (s)	84 (7) s	150 (20) s	200 (20) s
% rate increase	19 (10) %	22 (10) %	25 (10) %

[a]"ΔLag phase" is the change in lag phase from reactions with and without activator. Lag phase is the time from initiation of reaction to V_0. "% rate increase" is the increase in V_0 between reactions with and without activator. The error is displayed in parentheses.

Inhibitory and Allosteric Modulators Effect in the Presence of 1. ML351 is a selective, potent inhibitor of h15-LOX-1 that targets the active site.[24] The IC50 was determined in the presence of **1**; however, no change in the IC50 value was observed. This result suggests that any structural changes imparted to h15-LOX-1, as a result of **1** binding, does not change the active site affinity for ML351 in a quantifiable manner.

With respect to allostery, 14S-HpDHA is a known allosteric modulator of h15-LOX-1, where increasing concentrations affects the ratio of diHpDHA products being formed. With the addition of **1**, the allosteric effect of 14S-HpDHA on the diHpDHA metabolite ratio was unaffected, implying that the allosteric binding of **1** does not compete with that of 14S-HpDHA. 12S-HETE is also an allosteric modulator which regulates the substrate preference of h15-LOX-1 when reacting with AA and LA; however, **1** did not modify the allosteric effect of 12S-HETE either, indicating that **1** does not compete for the same binding site as 12S-HETE. Taken together, these data imply that the activation binding site of **1** is distinct from the binding site of both ML351 (i.e., the catalytic site[24]) and the allosteric effector molecules.[39−41] These data support the published hypothesis that **1** binds to a novel site on the exterior of h15-LOX-1.[8,31]

Steady-State Kinetic Analysis of 1. Given the fact that the AC_{50} values do not account for substrate concentration variations, steady-state kinetics with AA as the substrate were performed with 0, 5, 20, and 30 μM of **1** (Table 5). These studies determined that **1** did not affect K_M appreciably; however, **1** did increase k_{cat} and k_{cat}/K_m, in a hyperbolic, dose-dependent manner. This saturation behavior of k_{cat} and k_{cat}/K_M indicates hyperbolic activation (i.e., partial activation), comparable to the hyperbolic inhibition previously seen with h15-LOX-2 and 13S-HODE.[30] These data indicate the presence of an allosteric activation binding site that affects the catalysis by changing the microscopic rate constants of h15-LOX-1, as described in Scheme 2. From Scheme 2, eqs 1−4 allow for the determination of K_x (the strength of activator binding), α (the change in K_M) and β (the change in k_{cat}). As mentioned above, K_M is not affected by **1** indicating that the value of α is 1. If this value for α is inserted into eq 4, β and K_x can be determined from the fit to be 2.2 +/− 0.4 and 16 +/− 1 μM, respectively (Figure 10). These kinetic parameters indicate V-type activation[42] and the formation of a catalytically active ternary complex (X·E·S) between h15-LOX-1 and **1**, consistent with the proposed model of Meng et al.[8,31] It should be noted that the β value of 2.2 +/− 0.4 is consistent with the less accurate AC_{50} measurement for AA (242% max activation). In addition, the K_x is also similar to the measured AC_{50} value, with only a 2-fold difference.

CONCLUSIONS

The current work focused on the activity of compound **1** against h-LOX isoforms because they are important targets for the development of further understanding of the inflammatory response of human cells. Our continuing goal is to develop insights on small molecules that have action as both inhibitors and allosteric agents. Highlighted in the discussions presented

https://doi.org/10.1021/acsomega.2c05877
ACS Omega 2022, 7, 43169−43179

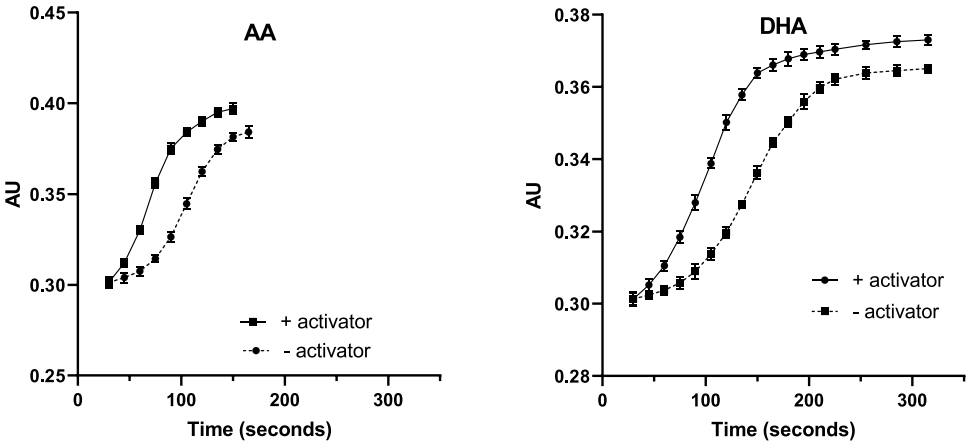

Figure 9. Lag phase activity plots of compound **1** with AA and h15-LOX-1 (left) and DHA and h15-LOX-1 (right). Time is in seconds and error is shown as bars for each measurement.

Table 5. Steady-State Kinetic Parameters with Activator (1) Present[a]

steady-state kinetics	0 μM	5 μM	20 μM	30 μM
k_{cat} (s^{-1})	9.1 (0.92)	12 (0.59) (+29%)	15 (0.90) (+65%)	16 (1.1) (+79%)
K_m (μM)	6.3 (2.6)	5.7 (0.75) (−8%)	5.6 (0.91) (−10%)	5.4 (1.3) (−14%)
k_{cat}/K_m (s^{-1} μM^{-1})	1.5 (0.021)	2.1 (0.026) (+41%)	2.7 (0.019) (+83%)	3.0 (0.030) (+107%)

[a] k_{cat} is in units of s^{-1}, K_m is in units of μM and k_{cat}/K_m is in units of s^{-1} μM^{-1}. Error values are in the parentheses, with % change from control boldened.

Scheme 2. Kinetic Scheme of Hyperbolic Activation with Concomitant Equations

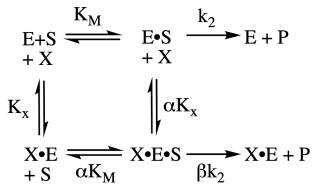

Equations:

$$1/v = (\alpha K_M/k_{cat})*[([X] + K_x)/(\beta[X] + \alpha K_x)]*1/[S]$$

$$+1/k_{cat}*[([X] + \alpha K_x)/(\beta[X] + \alpha K_x)] \quad (1)$$

$$K_M(app) = (\alpha K_M)*[([X] + K_x)/([X] + \alpha K_x)] \quad (2)$$

$$k_{cat}/K_M = (k_{cat}/\alpha K_M)*[(\beta[X] + \alpha K_x)/([X] + K_x)] \quad (3)$$

$$k_{cat} = k_{cat}*[(\beta[X] + \alpha K_x)/([X] + \alpha K_x)] \quad (4)$$

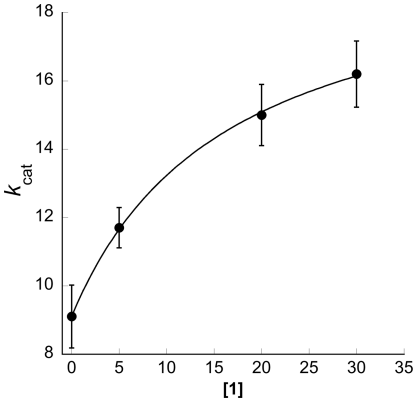

Figure 10. The k_{cat} apparent is plotted against increasing concentrations of **1** (μM) and fit to eq 4 from Scheme 2, resulting in β and K_x being 2.2 +/− 0.4 and 16 +/− 1 μM, respectively (α was set to 1).

above was that indazole-containing alkaloids (Figure 1) represent a privilege scaffold in the design of future anti-inflammation therapeutics. Our project successfully extended understanding on the ability of compound **1** (Figure 4) to function as a h-LOX activator, a phenomenon first discovered almost a decade ago by two other labs.[8,26,31] This project was launched to resolve some of the shortcomings in these previous studies, including (a) the incomplete description of the molecular structure of **1**, (b) the LOX constructs were challenged by mixtures the *trans*-**1** and *cis*-**1** isomers and not the individual compounds, and (c) details on the mechanism of action was poorly defined.

A key step in the project was the separation of the *trans*-**1**/*cis*-**1** obtained as distinct racemates from syntheses. Next, it was discovered that **1** (defined here as the *trans*/*cis* mixture) is active against h15-LOX-1; but inactive against h5-LOX, h12-LOX, and h15-LOX-2; demonstrating its action as a selective activator. Furthermore, the data collected showed that **1** activates h15-LOX-1 for LA and AA catalysis but not for DHA catalysis, indicating its action is dependent on the nature of the fatty acid substrate. The previous discovery that **1** reduced substrate inhibition was verified;[8] however, there is an additional complication. This effect was observed for both AA and DHA, and yet the rate of DHA is not activated; thus, the reduced substrate inhibition does not account for the activation by **1** of h15-LOX-1. In addition, **1** in this study did not compete with known catalytic and allosteric effector molecules, indicating that the binding site is unique to the known catalytic and allosteric locations, consistent with a conclusion previously proposed for **1**.[8,31] Finally, the outcomes obtained and discussed above demonstrate that **1** is a V-type activator, where K_M is not affected but k_{cat} is increased. This conclusion supports the hypothesis that the **1** binding site is remote from the catalysis site. In total, the data obtained during the study indicated that *trans*-**1** and *cis*-**1** are both

https://doi.org/10.1021/acsomega.2c05877
ACS Omega 2022, 7, 43169−43179

potent activators and that **1** (the *trans/cis* mixture) is selective to both its LOX target and its PUFA substrate affect. These observations further support the previous cellular work demonstrating that **1** is a tool molecule which increased the activity of h15-LOX-1 with respect to its LA/AA catalysis. However, **1** does not activate the reaction of h15-LOX-1 with DHA, indicating the need to discover an activator with broader specificity that could increase the production of DHA derived SPMs and possibly enhance the rate of inflammation resolution.

■ ASSOCIATED CONTENT

Supporting Information

The Supporting Information is available free of charge at https://pubs.acs.org/doi/10.1021/acsomega.2c05877.

General synthetic method. Figure S1. Proton and Carbon NMR of *trans*-**1**. Figure S2. Proton NOSEY NMR of *cis*-**1**. Figure S3. Proton NMR comparison with the literature. Figure S4. Carbon NMR comparison with the literature. General modeling method. Figure S5. Furan-Phenyl containing compound modeling. Figure S6. DiPhenyl containing compound modeling. Figure S7. AC_{50} of *cis*-**1** and *trans*-**1** (PDF)

■ AUTHOR INFORMATION

Corresponding Authors

Phillip Crews − *Department of Chemistry and Biochemistry, University of California Santa Cruz, Santa Cruz, California 95064, United States;* orcid.org/0000-0002-9061-9549; Email: pcrews@ucsc.edu

Theodore R. Holman − *Department of Chemistry and Biochemistry, University of California Santa Cruz, Santa Cruz, California 95064, United States;* orcid.org/0000-0001-8072-2959; Email: holman@ucsc.edu

Authors

Christopher van Hoorebeke − *Department of Chemistry and Biochemistry, University of California Santa Cruz, Santa Cruz, California 95064, United States*

Kevin Yang − *Department of Chemistry and Biochemistry, University of California Santa Cruz, Santa Cruz, California 95064, United States*

Samuel J. Mussetter − *Department of Chemistry and Biochemistry, University of California Santa Cruz, Santa Cruz, California 95064, United States*

Grant Koch − *Department of Chemistry and Biochemistry, University of California Santa Cruz, Santa Cruz, California 95064, United States*

Natalie Rutz − *Department of Chemistry and Biochemistry, University of California Santa Cruz, Santa Cruz, California 95064, United States*

R. Scott Lokey − *Department of Chemistry and Biochemistry, University of California Santa Cruz, Santa Cruz, California 95064, United States;* orcid.org/0000-0001-9891-1248

Complete contact information is available at: https://pubs.acs.org/10.1021/acsomega.2c05877

Notes

The authors declare no competing financial interest.

■ ACKNOWLEDGMENTS

The authors would like to thank Hsiau-Wei ("Jack") Lee, Ph.D. for acquiring the NMR data on various samples. We are grateful for the partial financial support for undergraduate research participants from NIH 2R25 GM051765 grant and for the UCSC ACCESS training program from Simpson Foundation PSB award.

■ ABBREVIATIONS

LOX, lipoxygenase
COX, cyclooxygenase
PUFAs, poly-unsaturated fatty acids
h5-LOX, human 5-lipoxygenase
h12-LOX, human platelet 12-lipoxygenase
h15-LOX-1, human 15-lipoxygenase-1
h15-LOX-2, human epithelial 15-lipoxygenase-2
AA, arachidonic acid
LA, linoleic acid
DHA, docosahexaenoic acid
HETE, hydroxyeicosatetraenoic acid
HODE, hydroxyoctadecadienoic acid
diHETE, dihydroxyeicosatetraenoic acid
diHpETE, dihydroperoxyeicosatetraenoic acid
diHDHA, dihydroxydocosahexaenoic acid
diHpDHA, dihydroperoxydocosahexaenoic acid
15S-HpETE, 15S-hydroperoxy-5*Z*,8*Z*,11*Z*,13*E*-eicosatetraenoic acid
15S-HpEPE, 15S-hydroperoxy-5*Z*,8*Z*,11*Z*,13*E*,17*Z*-eicosapentaenoic acid
14S-HpDHA, 14S-hydroperoxy-4*Z*,7*Z*,10*Z*,12*E*,16*Z*,19*Z*-docosahexaenoic acid
17S-HpDHA, 17S-hydroperoxy-4*Z*,7*Z*,10*Z*,13*Z*,15*E*,19*Z*-docosahexaenoic acid
12S-HETE, 12S-hydroxy-5*Z*,8*Z*,10*E*,14*Z*-eicosatetraenoic acid
12S-HpETE, 12S-hydroperoxy-5*Z*,8*Z*,10*E*,14*Z*-eicosatetraenoic acid
13S-HODE, 13S-hydroxy-9*Z*,11*E*-octadecadienoic acid
13S-HpODE, 13S-hydroperoxy-9*Z*,11*E*-octadecadienoic acid
SPM, specialized pro-resolving mediators
FA, formic acid
AC_{50}, activator concentration at 50% activation

■ REFERENCES

(1) Shrivastava, A.; Chakraborty, A. K.; Upmanyu, N.; Singh, A. Recent Progress in Chemistry and Biology of Indazole and its Derivatives: a Breif Reiew. *Austin J. Anal. Pharm. Chem.* **2016**, *3*, 1076.

(2) Elie, J.; Vercouillie, J.; Arlicot, N.; Lemaire, L.; Bidault, R.; Bodard, S.; Hosselet, C.; Deloye, J. B.; Chalon, S.; Emond, P.; Guilloteau, D.; Buron, F.; Routier, S. Design of selective COX-2 inhibitors in the (aza)indazole series. Chemistry, in vitro studies, radiochemistry and evaluations in rats of a [(18)F] PET tracer. *J. Enzyme Inhib. Med. Chem.* **2019**, *34*, 1−7.

(3) Polo-Cuadrado, E.; Acosta-Quiroga, K.; Rojas-Pena, C.; Rodriguez-Nunez, Y. A.; Duarte, Y.; Brito, I.; Cisterna, J.; Gutierrez, M. Molecular modeling and structural analysis of some tetrahydroindazole and cyclopentanepyrazole derivatives as COX-2 inhibitors. *Arabian J. Chem.* **2022**, *15*, 1−13.

(4) Minu, M.; Singh, D.; Mahaddalkar, T.; Lopus, M.; Winter, P.; Ayoub, A. T.; Missiaen, K.; Tilli, T. M.; Pasdar, M.; Tuszynski, J. Chemical synthesis, pharmacological evaluation and in silico analysis of new 2,3,3a,4,5,6-hexahydrocyclopenta[c]pyrazole derivatives as

potential anti-mitotic agents. *Bioorg. Med. Chem. Lett.* **2016**, *26*, 3855−3861.
(5) Minu, M.; Thangadurai, A.; Wakode, S. R.; Agrawal, S. S.; Narasimhan, B. Synthesis, antimicrobial activity and QSAR studies of new 2,3-disubstituted-3,3a,4,5,6,7-hexahydro-2H-indazoles. *Bioorg. Med. Chem. Lett.* **2009**, *19*, 2960−2964.
(6) Krapcho, J.; Turk, C. F. Bicyclic pyrazolines, potential central nervous system depressants and antiinflammatory agents. *J. Med. Chem.* **1979**, *22*, 207−210.
(7) Nasr, M. N.; Said, S. A. Novel 3,3a,4,5,6,7-hexahydroindazole and arylthiazolylpyrazoline derivatives as anti-inflammatory agents. *Arch. Pharm.* **2003**, *336*, 551−559.
(8) Meng, H.; McClendon, C. L.; Dai, Z.; Li, K.; Zhang, X.; He, S.; Shang, E.; Liu, Y.; Lai, L. Discovery of Novel 15-Lipoxygenase Activators To Shift the Human Arachidonic Acid Metabolic Network toward Inflammation Resolution. *J. Med. Chem.* **2016**, *59*, 4202−4209.
(9) Brash, A. R. Lipoxygenases: Occurrence, Functions, Catalysis and Acquisition of Substrate. *J. Biol. Chem.* **1999**, *274*, 23679−23682.
(10) Kuhn, H.; Banthiya, S.; van Leyen, K. Mammalian lipoxygenases and their biological relevance. *Biochim. Biophys. Acta* **2015**, *1851*, 308−330.
(11) Borgeat, P.; Samuelsson, B. Arachidonic acid metabolism in polymorphonuclear leukocytes: effects of ionophore A23187. *Proc. Natl. Acad. Sci. U. S. A.* **1979**, *76*, 2148−2152.
(12) Hamberg, M.; Samuelsson, B. Prostaglandin endoperoxides. Novel transformations of arachidonic acid in human platelets. *Proc. Natl. Acad. Sci. U. S. A.* **1974**, *71*, 3400−3404.
(13) Schewe, T.; Halangk, W.; Hiebsch, C.; Rapoport, S. M. A lipoxygenase in rabbit reticulocytes which attacks phospholipids and intact mitochondria. *FEBS Lett.* **1975**, *60*, 149−152.
(14) Brash, A. R.; Boeglin, W. E.; Chang, M. S. Discovery of a second 15S-lipoxygenase in humans. *Proc. Natl. Acad. Sci. U. S. A.* **1997**, *94*, 6148−6152.
(15) Wasternack, C.; Feussner, I. The Oxylipin Pathways: Biochemistry and Function. *Annu. Rev. Plant Biol.* **2018**, *69*, 363−386.
(16) Serhan, C. N.; Hamberg, M.; Samuelsson, B. Lipoxins: novel series of biologically active compounds formed from arachidonic acid in human leukocytes. *Proc. Natl. Acad. Sci. U. S. A.* **1984**, *81*, 5335−5339.
(17) Levy, B. D.; Clish, C. B.; Schmidt, B.; Gronert, K.; Serhan, C. N. Lipid mediator class switching during acute inflammation: signals in resolution. *Nat. Immunol.* **2001**, *2*, 612−619.
(18) Serhan, C. N.; Hong, S.; Gronert, K.; Colgan, S. P.; Devchand, P. R.; Mirick, G.; Moussignac, R. L. Resolvins: a family of bioactive products of omega-3 fatty acid transformation circuits initiated by aspirin treatment that counter proinflammation signals. *J. Exp. Med.* **2002**, *196*, 1025−1037.
(19) Serhan, C. N.; Petasis, N. A. Resolvins and protectins in inflammation resolution. *Chem. Rev.* **2011**, *111*, 5922−5943.
(20) Serhan, C. N. Pro-resolving lipid mediators are leads for resolution physiology. *Nature* **2014**, *510*, 92−101.
(21) Qu, Q.; Xuan, W.; Fan, G. H. Roles of resolvins in the resolution of acute inflammation. *Cell Biol. Int.* **2015**, *39*, 3−22.
(22) Carter, G. W.; Young, P. R.; Albert, D. H.; Bouska, J.; Dyer, R.; Bell, R. L.; Summers, J. B.; Brooks, D. W. 5-lipoxygenase inhibitory activity of zileuton. *J. Pharmacol. Exp. Ther.* **1991**, *256*, 929−937.
(23) Wenzel, S. E.; Kamada, A. K. Zileuton: the first 5-lipoxygenase inhibitor for the treatment of asthma. *Ann. Pharmacother.* **1996**, *30*, 858−864.
(24) Rai, G.; Joshi, N.; Jung, J. E.; Liu, Y.; Schultz, L.; Yasgar, A.; Perry, S.; Diaz, G.; Zhang, Q.; Kenyon, V.; Jadhav, A.; Simeonov, A.; Lo, E. H.; van Leyen, K.; Maloney, D. J.; Holman, T. R. Potent and selective inhibitors of human reticulocyte 12/15-lipoxygenase as anti-stroke therapies. *J. Med. Chem.* **2014**, *57*, 4035−4048.
(25) Offenbacher, A. R.; Holman, T. R. Fatty Acid Allosteric Regulation of C-H Activation in Plant and Animal Lipoxygenases. *Molecules* **2020**, *25*, 3374.
(26) Shintoku, R.; Takigawa, Y.; Yamada, K.; Kubota, C.; Yoshimoto, Y.; Takeuchi, T.; Koshiishi, I.; Torii, S. Lipoxygenase-mediated generation of lipid peroxides enhances ferroptosis induced by erastin and RSL3. *Cancer Sci.* **2017**, *108*, 2187−2194.
(27) Amagata, T. W. S.; Johnson, T. A.; Stessman, C. C.; Loo, C. P.; Lobkovsky, E.; Clardy, J.; Crews, P.; Holman, T. R. Exploring Sponge-Derived Terpenoids for Their Potency and Selectivity Against 12-Human, 15-Human, and 15-Soybean Lipoxygenases. *J. Nat. Prod.* **2003**, *66*, 230−235.
(28) Robinson, S. J.; Hoobler, E. K.; Riener, M.; Loveridge, S. T.; Tenney, K.; Valeriote, F. A.; Holman, T. R.; Crews, P. Using enzyme assays to evaluate the structure and bioactivity of sponge-derived meroterpenes. *J. Nat. Prod.* **2009**, *72*, 1857−1863.
(29) Smyrniotis, C. J.; Barbour, S. R.; Xia, Z.; Hixon, M. S.; Holman, T. R. ATP allosterically activates the human 5-lipoxygenase molecular mechanism of arachidonic acid and 5(S)-hydroperoxy-6(E),8(Z),11-(Z),14(Z)-eicosatetraenoic acid. *Biochemistry* **2014**, *53*, 4407−4419.
(30) Joshi, N.; Hoobler, E. K.; Perry, S.; Diaz, G.; Fox, B.; Holman, T. R. Kinetic and structural investigations into the allosteric and pH effect on the substrate specificity of human epithelial 15-lipoxygenase-2. *Biochemistry* **2013**, *52*, 8026−8035.
(31) Meng, H.; Dai, Z.; Zhang, W.; Liu, Y.; Lai, L. Molecular mechanism of 15-lipoxygenase allosteric activation and inhibition. *Phys. Chem. Chem. Phys.* **2018**, *20*, 14785−14795.
(32) Haasnoot, C. A. G.; Deleeuw, F. A. A. M.; Altona, C. The Relationship between Proton-Proton Nmr Coupling-Constants and Substituent Electronegativities .1. An Empirical Generalization of the Karplus Equation. *Tetrahedron* **1980**, *36*, 2783−2792.
(33) Gokhan-Kelekci, N.; Simsek, O. O.; Ercan, A.; Yelekci, K.; Sahin, Z. S.; Isik, S.; Ucar, G.; Bilgin, A. A. Synthesis and molecular modeling of some novel hexahydroindazole derivatives as potent monoamine oxidase inhibitors. *Bioorg. Med. Chem.* **2009**, *17*, 6761−6772.
(34) Khalaf, A. A.; El-Shafei, A. K.; El-Sayed, A. M. Synthesis of Some New Bicyclic Pyrazoline Derivatives. *J. Heterocyclic Chem.* **1982**, *19*, 609−612.
(35) Wecksler, A. T.; Jacquot, C.; van der Donk, W. A.; Holman, T. R. Mechanistic Investigations of Human Reticulocyte 15- and Platelet 12-Lipoxygenases with Arachidonic Acid. *Biochemistry* **2009**, *48*, 6259−6267.
(36) Lai, L.; Liu, Y.; Meng, H.; Hu, J. Hexahydroindazole 15-lipoxygenase activator and its application. Chinese patent #CN 105085401 A, 2015.
(37) Segraves, E. N.; Shah, R. R.; Segraves, N. L.; Johnson, T. A.; Whitman, S.; Sui, J. K.; Kenyon, V. A.; Cichewicz, R. H.; Crews, P.; Holman, T. R. Probing the activity differences of simple and complex brominated aryl compounds against 15-soybean, 15-human, and 12-human lipoxygenase. *J. Med. Chem.* **2004**, *47*, 4060−4065.
(38) Carroll, J.; Jonsson, E. N.; Ebel, R.; Hartman, M. S.; Holman, T. R.; Crews, P. Probing sponge-derived terpenoids for human 15-lipoxygenase inhibitors. *J. Org. Chem.* **2001**, *66*, 6847−6851.
(39) Wecksler, A. T.; Kenyon, V.; Deschamps, J. D.; Holman, T. R. Substrate specificity changes for human reticulocyte and epithelial 15-lipoxygenases reveal allosteric product regulation. *Biochemistry* **2008**, *47*, 7364−7375.
(40) Tsai, W. C.; Kalyanaraman, C.; Yamaguchi, A.; Holinstat, M.; Jacobson, M. P.; Holman, T. R. In Vitro Biosynthetic Pathway Investigations of Neuroprotectin D1 (NPD1) and Protectin DX (PDX) by Human 12-Lipoxygenase, 15-Lipoxygenase-1, and 15-Lipoxygenase-2. *Biochemistry* **2021**, *60*, 1741−1754.
(41) Freedman, C.; Tran, A.; Tourdot, B. E.; Kalyanaraman, C.; Perry, S.; Holinstat, M.; Jacobson, M. P.; Holman, T. R. Biosynthesis of the Maresin Intermediate, 13S,14S-Epoxy-DHA, by Human 15-Lipoxygenase and 12-Lipoxygenase and Its Regulation through Negative Allosteric Modulators. *Biochemistry* **2020**, *59*, 1832−1844.
(42) Reinhart, G. D. Quantitative analysis and interpretation of allosteric behavior. *Methods Enzymol.* **2004**, *380*, 187−203.

https://doi.org/10.1021/acsomega.2c05877
ACS Omega 2022, 7, 43169−43179